ESTIMATION OF SPACEBORNE LIDAR SYSTEM POTENTIALITIES FOR SEA WATER SOUNDING

G.M Krekov, M.M. Krekova, G.G. Matvienko, and V.S. Shamanaev

Siberian State Medical University
Institute of Atmospheric Optics,
Siberian Branch of the Russian Academy of Sciences, Tomsk
Received November 23, 1995

Results of calculations of the amplitude and shape of a signal of a spaceborne lidar operating in the system atmosphere–ocean are presented in the paper. The calculations have been done by the Monte Carlo method for wavelength $\lambda = 0.53$ μm. *The dependence of the lidar return signal characteristics on the atmospheric optical state, water–air interface, and optical properties of sea water has been studied. A signal from the atmosphere is shown to mask completely a signal from a subsurface water layer.*

Spaceborne lidar systems are coming into practical use in scientific researches as well as in solving ecological, meteorological, and some other problems. Results of theoretical investigations of the possibility of using lidar systems for the study of optical properties of a subsurface water layer and for bathymetry are presented in this paper.

1. FORMULATION OF THE PROBLEM

In our papers published earlier[1,2] we considered the efficiency of a lidar system placed on board an aircraft flying at altitudes 200–300 m above the water surface. The influence of different factors including stochastic interface and atmospheric aerosol on lidar return signal shape was considered. It was revealed that the wind-driven sea waves caused the losses of lidar signal energy recorded in a finite time. Optimizing the receiving angle of view, it is possible to decrease these losses. A waveform of a lidar return signal also depends on the state of the interface. For the entire measurement time, the increase of the wind velocity results in the decrease of the signal amplitude.

The influence of the atmosphere is manifested through limited sounding depth. This occurs when a signal from the atmosphere caused by radiation scattering, reflection, and re-reflection from the interface is superimposed on a signal reflected by the water medium. Depending on the distance from a lidar to the interface, optical depth of water, and receiving angle of view the sounding depth is 50–70 m.

It is evident that moving the lidar system away at a considerable distance from an object of sounding results in the increase of a viewing cone volume. Because of this, the influence of the atmosphere on lidar return signal waveform may substantially increase. The degree of this influence can hardly be predicted and so the precise estimation is needed.

2. METHOD OF SOLUTION

The results of numerical simulation performed by the Monte Carlo method are presented below. This method was chosen because it allows one to assess separately the contribution of different factors in the process of reflected signal shaping.

It was assumed that a monostatic laser radar with the optical axis oriented in the nadir was at a distance of 300 km from the air–water interface. A transmitter and a receiver had circular apertures of unit radii. The isotropic transmitter radiated a δ-pulse within a solid angle Ω_t with an apex angle φ_t and a reflected signal was recorded by the receiver within a solid angle Ω_r with an apex angle φ_r. Here, $1/2\,\varphi_t$ was taken 0.1 mrad and the receiving angle of view varied in the range $0.1 \le \varphi_r \le 1.7$ mrad. It was assumed that the interface was rough and stochastic, i.e., the water surface was an ensemble of randomly oriented micropatches the normals to which had a probability density function $P(s)$ described by the truncated two-dimensional distribution density of tilts z_x and z_y

$$P(s) = P(z_x, z_y) =$$
$$= 2\pi(\sigma_x \sigma_y)^{-1}\exp\{-(z_x/\sigma_x)^2/2 - (z_y/\sigma_y)^2/2\},$$

where $z_x = S_x/S_z$ and $z_y = S_y/S_z$, S_x and S_y are the projections of normal $\mathbf{S}$ on the z axis. The standard deviations of tilts depend on the wind speed V as[3]

$$\sigma_x = 0.0031V,\ \sigma_y = 0.003 + 0.00192V.$$

Optical properties of the sea water were specified allowing for its multicomponent structure, with the parameters borrowed from the literature (see, for example, Ref. 4). Calculations were performed for the scattering phase functions of two types given in Table I.

0235-6880/96/05 396-04 $02.00

TABLE I.

ϑ, °	g_1	g_2	ϑ, °	g_1	g_2	ϑ, °	g_1	g_2
0	2789.75	565.47	50	0.043	0.141	120	0.0061	0.025
5	32.799	34.096	60	0.0138	0.079	130	0.0063	0.026
10	4.42	9.103	70	0.0092	0.049	140	0.0066	0.023
15	0.464	3.505	80	0.0077	0.032	150	0.0068	0.041
20	0.899	2.035	90	0.0066	0.026	160	0.0069	0.049
30	0.189	0.678	100	0.0062	0.023	170	0.0069	0.052
40	0.097	0.282	110	0.0059	0.023	180	0.007	0.053

The scattering phase function $g_1(\vartheta)$ is characteristic of the open ocean water where organic particles are predominant, and $g_2(\vartheta)$ is more characteristic of shallow water regions and drifts of rivers where mineral particles dominate. The distinctive feature of $g_2(\vartheta)$ is its less pronounced asymmetry and higher values at angles close to 180°. In calculations the absorptive properties of the sea water were characterized by the probability of photon survival ω. Vertical distribution of the radiation attenuation coefficient in the atmosphere was specified according to Refs. 5 and 6. The albedo of the bottom was taken 0.2.

We calculated the components of a signal

$$I(h) = I_a(h)+I_w(h)+I_b(h),$$

where $h = v_i t$ is the distance to the lidar system that depends on time t of radiation arrival at the detector, v_i is the speed of light in the atmosphere or in the water, $I(h)$ is the resultant signal recorded by the detector, $I_a(h)$ is its atmospheric component due to scattering on aerosol particles and reflection from the air–water interface, $I_w(h)$ is the component reflected from a subsurface water layer, and $I_b(h)$ is the signal component reflected from the bottom.

3. INFLUENCE OF LIDAR PARAMETERS

Results of $I(h)$ calculations for waters of average productivity with $\sigma_w = 0.18$ m^{-1}, $g_1(\vartheta)$, and $\omega = 0.83$ are shown in Fig. 1. The data are shown for $1/2\ \varphi_r = 0.8$ and 1.7 mrad. At smaller angles φ_r the dynamic range of a signal becomes very wide, while the increase of $1/2\ \varphi_r$ up to the values larger than 1.7 mrad also makes no sense because of insignificant change of the signal $I(h)$. Thus, a signal is completely shaped at the angular aperture of the receiver $1/2\ \varphi_r \sim 2$ mrad. The data shown in Fig. 2 clearly indicate that the behavior and value of the signal $I(h)$ are primarily determined by its atmospheric component $I_a(h)$.

In the first intervals (to depths as great as 10 m) the signal $I_a(h)$ exceeds $I_w(h)$ almost by two orders of magnitude, then their difference decreases to an order of magnitude. It should be noted that bathymetry is still possible at $1/2\ \varphi_r < 2$ mrad. If the angular aperture becomes larger than 2 mrad, the atmospheric component of the signal $I_a(h)$ fully masks the signal $I_b(h)$ reflected from the bottom.

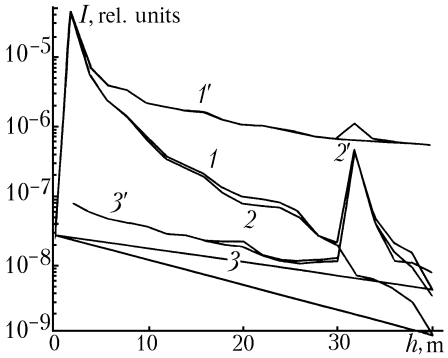

FIG. 1. Dependence of the signal amplitude $I(h)$ and its components $I_a(h)$ and $I_w(h)$ on the depth of a sounded layer. Curves 1, 2, and 3 are for $I(h)$, $I_a(h)$, and $I_w(h)$ at $1/2\ \varphi_r = 0.8$ mrad, curves 1′, 2′, and 3′ – at $1/2\ \varphi_r = 1.7$ mrad.

High intensity of the atmospheric signal is caused by multiple scattering of radiation in the processes of its reflection and re-reflection and by accumulation of the path lengths of photons on the periphery of the source cone before their arrival at the interface. Radiation scattered in the boundary layer of the atmosphere also contributes to the signal intensity.

It should be noted that in all figures of this article the atmospheric component $I_a(h)$ is shown from the instant of arrival of radiation reflected from a subsurface layer.

4. INFLUENCE OF THE WIND SPEED

The data shown in Fig. 1 were calculated for the driving wind speed $V = 1$ m/s. The atmospheric component $I_a(h)$ is slightly influenced by changes of the wind speed; at the same time, the values of $I_w(h)$ can change considerably. In Fig. 2 curves *1* and *2* show the signal $I_a(h)$ and curves *3* and *4* – the signal $I_w(h)$ for wind speed $V = 1$ and 3 m/s, respectively. Our calculations were done for the receiving angles $1/2\ \varphi_r = 0.8$ mrad. Analysis of the results obtained for different values of the wind speed revealed that the increase of V causes the decrease of $I_w(h)$ with depth;

the maximum $I_b(h)$ also decreases. Detection of the signal $I_b(h)$ for $V = 7$ m/s is still possible but only for angular apertures $1/2\ \varphi_r < 1$ mrad.

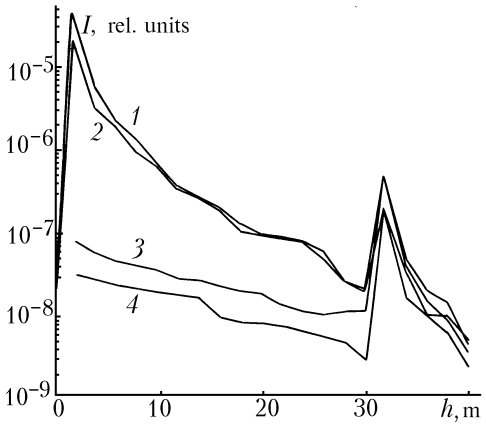

FIG. 2. Amplitudes of signals $I_a(h)$ and $I_w(h)$ vs. the speed of near-surface wind. Curves 1 and 2 are for $I_a(h)$, 3 and 4 – for $I_w(h)$. $V = 1$ (1 and 3) and 3 m/s (2 and 4).

5. INFLUENCE OF THE PARAMETERS OF WATER

Optical depth of water σ_w is often higher than that assumed in calculations described above. It may reach 0.3–0.4 m^{-1} in productive regions. Results obtained for $\sigma_w = 0.3$ m^{-1} and $\omega = 0.86$ are shown in Fig. 3 for angles $1/2\ \varphi_r = 1.7$ mrad. The increase of water optical depth also influences weakly the resultant signal $I(h)$; only the qualitative behavior and amplitude of the signal $I_w(h)$ are changed. In Fig. 3, signals $I_w(h)$ (curves *1* and *2*) and $I(h)$ (curves *3* and *4*) are shown as functions of h for $\sigma = 0.18$ and 0.3 m^{-1}. The increase of optical depth results in the slight increase of $I_w(h)$ in the first intervals and then the level of $I_w(h)$ decreases resulting in the decrease of the maximum $I_b(h)$. Obviously the increase of the optical depth of water makes the detection of $I_b(h)$ more difficult, but with smaller angular apertures φ_r it is still possible. In the example considered above reliable detection of $I_b(h)$ is possible at angles $1/2\ \varphi_r < 2$ mrad.

The estimates discussed above were obtained for the sea water with the high concentration of organic particles and highly asymmetric scattering phase function. The increase of the mineral fraction concentration changes the optical properties of water: the scattering phase function becomes less asymmetric and probability of radiation scattering at angles close to π also increases (compare the values of $g_1(\vartheta)$ and $g_2(\vartheta)$ presented in Table I).

Results obtained for the scattering phase function $g_2(\vartheta)$ are shown in Fig. 4. Functions $I_w(h)$ (curves *1* and *2*) and $I(h)$ (curves *3* and *4*) were obtained for the receiving field-of-view angle $1/2\varphi_r = 0.8$ mrad and the scattering phase functions g_1 and g_2, respectively. In calculations with $g_2(\vartheta)$ the dependence of the signal $I(h)$ on the amplitude of the signal $I_w(h)$ was observed.

At depths greater than $h \sim 5$ m the amplitudes of $I_w(h)$ and $I(h)$ are of the same order, with the further increase of depth curves $I_w(h)$ and $I(h)$ come closer because the signals $I_a(h)$ and $I_w(h)$ become comparable. It should be noted that for these input parameters the relative level of the maximum $I_b(h)$ is slightly lowered. Allowing for the fact that $g_2(\vartheta)$ is more typical of coastal and shallow waters characterized by high optical depths, it can be seen that with $g_2(\vartheta)$ the level of $I_w(h)$ becomes even higher especially at low depths (see Fig. 3). It seems likely that in this case the component $I_a(h)$ may be separated from the signal $I(h)$. The method of separation should be considered specially.

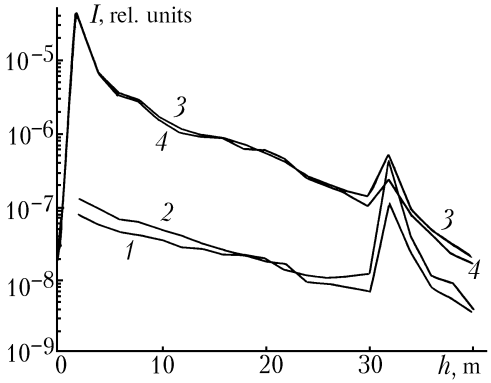

FIG. 3. Influence of the sea water optical depth on the amplitude of signals $I_w(h)$ (curves 1 and 2) and $I(h)$ (3 and 4). Here, $\sigma_w = 0.18$ (1 and 3) and 0.3 m^{-1} (2 and 4), $1/2\ \varphi_r = 1.7$ mrad.

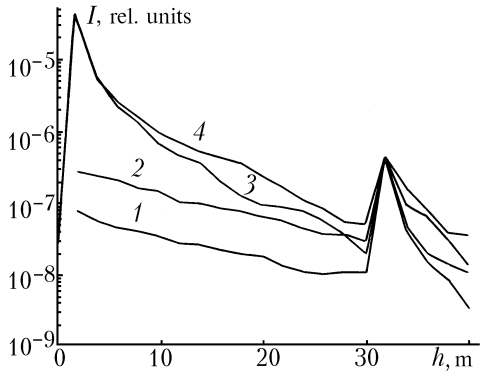

FIG. 4. Influence of the sea water scattering properties on the signal waveform. Curves 1 and 2 are for $I_w(h)$, 3 and 4 – for $I(h)$. The values of the scattering phase function $g_1(\vartheta)$ (curves 2 and 4) were taken from Table I. Here, $1/2\ \varphi_r = 0.8$ mrad, $V = 1$ m/s, and $\sigma_w = 0.18$ m^{-1}.

6. INFLUENCE OF THE ATMOSPHERIC PARAMETERS

Calculated results for the atmospheric signal component $I_a(h)$ discussed above were obtained assuming that the scattering properties of the atmosphere correspond to Deirmendjian's H haze.[6] Results of numerous recent investigations into microphysics and microstructure of the atmosphere above the rough oceanic surface were systematized in Ref. 5. In this paper, it was also pointed out that due to peculiarities of aerosol particle origin, the particle size distribution function is polymodal and differs considerably from the four-parametric representation.[6] This difference is caused primarily by the presence of large and submicron particles in the atmosphere that cause redistribution of scattered radiation into the forward and backward hemispheres. The model scattering phase matrix, allowing for the properties of the surface atmospheric layer above the ocean, was proposed in Ref. 5. This model was used in the next series of our calculations. Table II compares the values of two scattering phase functions of the atmosphere above the ocean used in our calculations.

TABLE II.

ϑ, °	g_3	g_4	ϑ, °	g_3	g_4
0	48.69	200.69	90	0.052	0.065
5	23.27	53.1	100	0.0416	0.054
10	9.7	2.341	110	0.037	0.048
15	5.13	1.62	120	0.039	0.035
20	3.14	1.21	130	0.049	0.029
30	1.39	0.711	140	0.0711	0.044
40	0.679	0.572	150	0.0879	0.049
50	0.353	0.433	160	0.097	0.051
60	0.195	0.259	170	0.126	0.053
70	0.116	0.105	180	0.161	0.062
80	0.074	0.085			

It should be noted that all the results shown in Figs. 1–4 were calculated with the scattering phase function $g_3(\vartheta)$. Calculated results for the atmospheric signal component with the scattering phase function $g_4(\vartheta)$ are shown in Fig. 5. Curves *1* and *4*, *2* and *5*, and *3* and *6* are for signals $I_w(h)$, $I_a(h)$, and $I(h)$ at angles $1/2\,\varphi_r = 0.8$ and 1.75 mrad, respectively. The other parameters are $\sigma_w = 0.18\ m^{-1}$, $\omega = 0.83$, and $V = 1$ m/s. At depths greater than ~10 m, $I_a(h)$ and $I_w(h)$ are of the same order. It should be emphasized that according to our calculations, the waveform of the signal $I_a(h)$ superimposed on the signal $I_w(h)$ is influenced primarily by the lower atmospheric layer of high optical thickness. Using this peculiarity, it is possible to separate the atmospheric component of a signal, for example, when two different wavelengths are used for sounding and one of them is absorbed by the sea water. This is possible if the optical characteristics of the surface atmospheric layer at the given wavelengths are correlated.

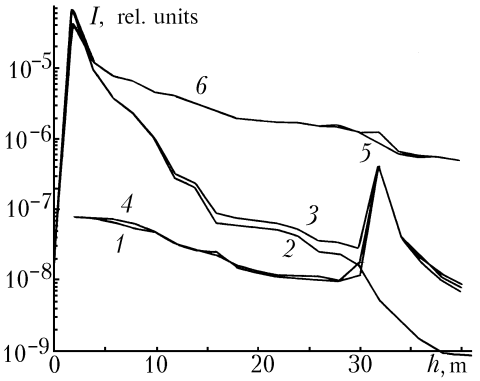

FIG. 5. Components of the lidar return signal $I(h)$ calculated with the scattering phase function of the atmosphere above the ocean $g_4(\vartheta)$ given in Table II. Curves 1 and 4 are for $I_w(h)$, 2 and 5 – for $I_a(h)$. Here, $1/2\,\varphi_r = 0.8$ (1, 2, and 3) and 1.75 mrad (4, 5, and 6), $\sigma_w = 0.18\ m^{-1}$, and $V = 1$ m/s.

7. CONCLUSION

On the basis of our investigations, it is possible to conclude that the atmosphere and especially its boundary layer distort considerably lidar return signals in laser sounding of subsurface layers of water media and objects in water. The field of view of a lidar telescope must be less than 4 mrad. When the sea surface is rough, lidar signals reflected by water depth and by the bottom become weaker. The increase of the water optical depth results in the increase of the component of a lidar signal recorded from low water depths (5–10 m), at greater depths this component decreases. A signal reflected from the bottom also decreases. The amplitude of lidar return signals depends on the scattering phase function of the water medium. The increase of the signal amplitude is observed for less asymmetric scattering phase function. The method to assess the contribution of the atmosphere to the lidar signal reflected from the bottom and from the water depth has been proposed. In this method, sounding is performed at two wavelengths one of which is absorbed by water.

REFERENCES

1. B.A. Kargin, G.M. Krekov, and M.M. Krekova, Atmos. Oceanic Opt. **5**, No. 3, 191–195 (1992).
2. G.M. Krekov, M.M. Krekova, and V.S. Shamanaev, Atmos. Oceanic Opt. **5**, No. 11, 777–779 (1992).
3. C. Cox and W. Munk, J. Opt. Soc. Am. **44**, No. 11, 838 (1954).
4. O.V. Kopelevich and K.S. Shifrin, in: *Oceanic and Atmospheric Optics* (Nauka, Moscow, 1981), p. 4.
5. G.M. Krekov and R.F. Rakhimov, *Optical Models of the Atmospheric Aerosol* (Institute of Atmospheric Optics of the Siberian Branch of the Academy of Sciences of the USSR, Tomsk, 1986), 294 pp.
6. D. Deirmendjian, *Electromagnetic Scattering on Spherical Polydispersions* (Elsevier, Amsterdam,1969).